Contents lists available at ScienceDirect

Journal of Computational Physics

journal homepage: www.elsevier.com/locate/jcp

A comparative study of the delta-Eddington and Galerkin quadrature methods for highly forward scattering of photons in random media

Hiroyuki Fujii[a,*], Go Chiba[b], Yukio Yamada[c], Yoko Hoshi[d], Kazumichi Kobayashi[a], Masao Watanabe[a]

[a]*Division of Mechanical and Space Engineering, Faculty of Engineering, Hokkaido University, Kita 13 Nishi 8, Kita-ku, Sapporo, Hokkaido 060-8628, Japan*
[b]*Division of Energy and Environmental Systems, Faculty of Engineering, Hokkaido University, Kita 13 Nishi 8, Kita-ku, Sapporo, Hokkaido 060-8628, Japan*
[c]*Center for Neuroscience and Biomedical Engineering, University of Electro-Communications, 1-5-1 Chofugaoka, Chofu, Tokyo 182-8585, Japan*
[d]*Preeminent Medical Photonics Education & Research Center, Hamamatsu University School of Medicine, 1-20-1 Handayama, Higashi-ku, Hamamatsu, Sizuoka 431-3192, Japan*

ARTICLE INFO

Article history:

Keywords: Radiative transfer theory, Highly forward-peaked phase function, Discrete ordinates method, Legendre polynomial expansion, Weighting procedure

ABSTRACT

A versatile and accurate treatment for the highly forward-peaked phase function in the three-dimensional (3D) radiative transfer equation (RTE) based on the discrete ordinates method (DOM) is crucial for biomedical optics. Our first objective was to compare the delta-Eddington (dE) and Galerkin quadrature (GQ) methods. The dE method decomposes the phase function into a purely forward-peaked component and the other component, and expands the other component by Legendre polynomials as well as the finite order Legendre expansion (FL) method does. The GQ method conducts the weighting procedure in addition to the Legendre expansion. Although it was reported that both methods can provide the accurate results for calculations of the RTE, the versatility of both methods is still unclear.

The second objective was to examine a possibility of a conjunction of the GQ method with the dE method, called as the GQ-dE method, which has the advantages of both methods. We examined numerical errors in the moment conditions of the phase function using the FL, dE, GQ, and GQ-dE methods at various types and orders of the quadrature sets, mainly in the region of the errors induced by the angular discretization using the DOM. The errors were reduced by the dE method from those by the FL method, however the error reduction depended on the types and orders of the quadrature sets. Meanwhile, the errors were significantly reduced by the GQ and GQ-dE methods, regardless of the quadrature sets. We also verified the numerical calculations of the time-dependent 3D RTE by the analytical solution of the RTE for homogeneous media in the region of the scattering length scale, where the highly forward-peaked phase function strongly influences the RTE-results. The errors in the RTE-results were similar to those in the moment conditions. Our results suggest the higher versatility and accuracy of the GQ and GQ-dE methods than those of the FL and dE methods.

1. Introduction

Various kinds of random media such as biological tissue volumes and agricultural products scatter photons strongly in the highly forward direction (Cheong et al., 1990; Baranyai and Zude, 2009). Clarification of the highly forward-peaked scattering of photons is crucial in application fields of biomedical imaging and postharvest technology (Gibson et al., 2005; Okawa et al., 2011; Kannan and Przekwas, 2011; Yamada and Okawa, 2014; Hoshi and Yamada, 2016). Photon transport in the random media is governed by the radiative transfer equation (RTE) and the highly forward-peaked scattering of photons is expressed by a phase function in the scattering integral term of the RTE. There exist three kinds of characteristic length scales on photon transport: the ballistic, scattering, and diffusive length scales corresponding to short, medium, and long source-detector (SD) distances, respectively. In the region of the scattering length scale, photon transport is strongly influenced by the highly forward-peaked phase function, while in the regions of the other two length scales, the shape of the phase function little influences photon transport. In this paper, we mainly consider photon transport in the region of the scattering length scale.

Usually, the RTE is solved numerically rather than analytically because the random media are generally heterogeneous, while the analytical solutions of the RTE are obtained mainly for homogeneous media. For angular discretization in numerical calculations of the RTE, the discrete ordinates method (DOM) is one of the gold standards, which calculates the scattering integral as a quadrature sum with a quadrature set: discrete angular directions and their weights. Despite the success of the DOM for isotropic or weakly anisotropic scattering, accurate and efficient calculations of the RTE for highly forward-peaked scattering are still challenging. Because for highly forward-peaked scattering, the phase function changes exponentially as a function of the scattering angle, numerical errors of the moment conditions of the phase function become larger than those for isotropic or weakly anisotropic scattering. The numerical errors of the moment conditions lead to large numerical errors of the RTE-calculations for highly forward-peaked scattering.

To overcome the difficulty, various kinds of numerical treatments of the highly forward-peaked phase function based on the DOM have been extensively developed in the different research fields (Joseph et al., 1976; Welch and van Gemert, 1995; Klose et al., 2005; Liu et al., 2002; Hunter and Guo, 2012; Long et al., 2016; Fujii et al., 2016; Morel, 1989; Morel et al., 2017; Fujii et al., 2018), which are roughly categorized into the two types. The first type is based on an expansion of the phase function by a finite series of Legendre polynomials, such as the finite order Legendre expansion (FL) and the delta-Eddington (dE) methods (Joseph et al., 1976; Welch and van Gemert, 1995). Here, we define the FL method as a method which simply expands the phase function, while the dE method decomposes the phase function into purely forward-peaked and other components, and then expands the other component. Thanks to the orthogonality of the polynomials, the numerical errors of the moment conditions are reduced. The dE method has been widely used in the field of biomedical optics (Klose et al., 2005; Jia et al., 2015) since the introduction

*Corresponding author. He partially conducted this research while he was a visiting scholar at University of Michigan.

by Klose and coworkers (Klose and Hielscher, 2003) from the field of astrophysics. Nevertheless, the validity and versatility are still unclear. Klose et al. reported that the second order dE method can provide accurate calculations of the RTE for highly forward-peaked scattering although in the only one case of a quadrature set (Klose et al., 2005). Jia et al. stated the zeroth order is sufficient (Jia et al., 2015), however, they discussed in the region of the diffusive length scale, where the phase function little influences the RTE-calculations. Hence, it is still required to examine the dE method. The other type is based on a weighting procedure of the phase function so as to satisfy the moment conditions, such as the renormalization methods of the phase function (Liu et al., 2002; Hunter and Guo, 2012; Fujii et al., 2016). Although the first order renormalization method can provide accurate results of the RTE, a preliminary investigation for an adequate choice of the quadrature set is necessary because the accuracy of the RTE-calculations using the weighting procedure depends on the type and order of the quadrature sets.

The Galerkin quadrature (GQ) method, originally developed in the field of charged-particle transport (Morel, 1989; Morel et al., 2017), takes the advantages of both types: this method expands the phase function by Legendre polynomials and conducts the weighting procedure consistently in Galerkin's way, which is popular for the finite element method. The GQ method ensures that the discrete scattering integral is accurate, regardless of the convergence of the truncated expansion of the phase function by Legendre polynomials. Recently, the GQ method was firstly employed in the field of biomedical optics and compared with the first order renormalization method (Fujii et al., 2018). It was shown that this method can provide accurate calculations of the RTE as well as the renormalization method can, although the comparison study was investigated in the only one case of a quadrature set. For the GQ method, the accuracy of the RTE-solution only depends on the adequacy of the quadrature set for representing the light intensity. Hence, it is necessary to examine the dependence of the numerical calculations of the RTE using the GQ method on the quadrature sets.

One of our objectives was to numerically examine the versatility and accuracy of the dE and GQ methods for the RTE-calculations for highly forward-peaked scattering with various kinds and orders of quadrature sets by comparing with the FL method as a reference. The comparison study of the three methods allows us to examine the effects of two types of treatments separately; one is the Legendre expansion of the phase function and the other is the weighting procedure for highly forward-peaked scattering.

The other objective was to examine a possibility of a conjunction of the Galerkin method with the dE method, called as the GQ-dE method, which probably has advantages of both the methods. Firstly, we investigated the numerical errors in the moment conditions of the phase function using the four methods (FL, dE, GQ, and GQ-dE methods). Then, we investigated the numerical calculations of the time-dependent RTE using the four methods in the region of the scattering length scale for three-dimensional (3D) random media.

The following section describes the RTE as a photon transport model in 3D random media. Sections 3 and 4 provide the numerical treatments of highly forward-peaked phase function based on the DOM, and the numerical schemes and conditions for the RTE-calculations. Section 5 provides the numerical results of the moment conditions of the phase function and the RTE-calculations for highly forward-peaked scattering, and examine the versatility and accuracy of the FL, dE, GQ, and GQ-dE methods. Finally, conclusions are described.

2. Photon transport model

2.1. Radiative transfer equation (RTE)

The time-dependent RTE is formulated for 3D random media (Chandrasekhar, 1960) as

$$\left[\frac{\partial}{v\partial t} + \mathbf{\Omega}\cdot\nabla + \mu_a(\boldsymbol{r}) + \mu_s(\boldsymbol{r})\right] I(\boldsymbol{r},\mathbf{\Omega},t) = \mu_s(\boldsymbol{r})\int_{\mathbb{S}^2} d\mathbf{\Omega}'\, p(\mathbf{\Omega},\mathbf{\Omega}')I(\boldsymbol{r},\mathbf{\Omega}',t) + q(\boldsymbol{r},\mathbf{\Omega},t), \tag{1}$$

where $I(\boldsymbol{r},\mathbf{\Omega},t)$ in W cm^{-2} sr^{-1} represents the light intensity as a function of spatial position $\boldsymbol{r} = (x,y,z) \in \mathbb{R}^3$ in cm; angular direction (unit direction vector) $\mathbf{\Omega} = (\Omega_x,\Omega_y,\Omega_z) \in \mathbb{S}^2$ in sr; and time t in ps. $\mu_a(\boldsymbol{r})$ and $\mu_s(\boldsymbol{r})$ in cm^{-1} are the absorption and scattering coefficients, respectively; v is the speed of light in the medium; $p(\mathbf{\Omega},\mathbf{\Omega}')$ in sr^{-1} is the phase function with $\mathbf{\Omega}$ and $\mathbf{\Omega}'$ denoting the scattered-in and -out directions, respectively; and $q(\boldsymbol{r},\mathbf{\Omega},t)$ in W cm^{-3} sr^{-1} is a source function. The first term of the right hand side of Eq. (1) is called as the scattering integral, which describes energy gain of photons by scattering.

2.1.1. Henyey-Greenstein (HG) phase function and anisotropy factor

For a formulation of $p(\mathbf{\Omega},\mathbf{\Omega}')$, the Henyey-Greenstein (HG) phase function (Henyey and Greenstein, 1941) is widely employed in biomedical optics as a mathematical model (not as a physical model):

$$p_{HG}(\mathbf{\Omega}\cdot\mathbf{\Omega}') = \frac{1}{4\pi}\frac{1-g^2}{(1+g^2-2g\mathbf{\Omega}\cdot\mathbf{\Omega}')^{3/2}}, \tag{2}$$

where $g \in$[-1, 1] is the anisotropy factor, defined as the average cosine, $\mathbf{\Omega}\cdot\mathbf{\Omega}'$, over a whole solid angle. The g-values of biological tissue volumes are typically larger than 0.8 (Cheong et al., 1990), meaning the highly forward-peaked scattering. In Fig. 1, the HG phase functions (Eq. (2)) at several g-values are plotted as a function of $\mathbf{\Omega}\cdot\mathbf{\Omega}' \in [-1,1]$ in a logarithmic scale. As the g-value approaches to unity, the exponential change of p_{HG} with respect to $\mathbf{\Omega}\cdot\mathbf{\Omega}'$ becomes enhanced and the peak of p_{HG} around $\mathbf{\Omega}\cdot\mathbf{\Omega}' = 1.0$ becomes sharp. In this paper, we mainly consider the g-value to be 0.9.

The HG phase function can be expanded in the infinite series of (unassociated) Legendre polynomials, P_L ($L = 0, 1, \cdots, \infty$):

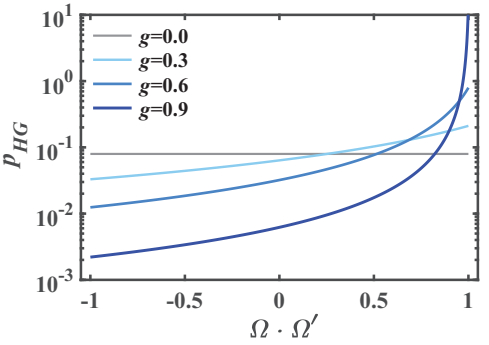

Fig. 1. HG phase function, p_{HG} (Eq. (2)), as a function of $\mathbf{\Omega}\cdot\mathbf{\Omega}'$ in a logarithmic scale at several g-values. (For interpretation of the colors in the figure(s), the reader is referred to the web version of this article.)

$$p_{HG}(\mathbf{\Omega}\cdot\mathbf{\Omega}') = \sum_{L=0}^{\infty} \frac{2L+1}{4\pi} \sigma_{L,\,HG} P_L(\mathbf{\Omega}\cdot\mathbf{\Omega}'). \tag{3}$$

The expansion coefficient, $\sigma_{L,\,HG}$, is given by

$$\sigma_{L,\,HG} := \int_{\mathbb{S}^2} d\mathbf{\Omega}' p_{HG}(\mathbf{\Omega}\cdot\mathbf{\Omega}') P_L(\mathbf{\Omega}\cdot\mathbf{\Omega}') = g^L. \tag{4}$$

The above equation is also called as the L-th order moment condition of the phase function. The case of $L = 0$ corresponds to the normalization condition of the phase function: $\int_{\mathbb{S}^2} d\mathbf{\Omega}' p_{HG}(\mathbf{\Omega}\cdot\mathbf{\Omega}') = 1$.

3. Numerical treatments of the highly forward-peaked scattering

3.1. Discrete ordinates method (DOM)

For angular discretization, we employed the DOM, which approximates the scattering integral as a quadrature sum:

$$\mu_s(\boldsymbol{r}) \int_{\mathbb{S}^2} d\mathbf{\Omega}' p(\mathbf{\Omega}\cdot\mathbf{\Omega}') I(\boldsymbol{r},\mathbf{\Omega}',t) \sim \mu_s(\boldsymbol{r}) \sum_{l'=1}^{N_\Omega} w_{l'} p_{ll'} I_{l'}(\boldsymbol{r},t), \tag{5}$$

where subscripts l and $l' \in [1, 2, \cdots N_\Omega]$ denote the indices of the discrete angular directions, $\mathbf{\Omega}_l$ and $\mathbf{\Omega}_{l'}$, respectively; N_Ω is a total number of the discrete angular directions; $w_{l'}$ is a weight for numerical integration; and $p_{ll'} = p(\mathbf{\Omega}_l\cdot\mathbf{\Omega}_{l'})$ is a discrete form of the phase function. The L-th order moment condition of the phase function (Eq. (4)) is also discretized as

$$\int_{\mathbb{S}^2} d\mathbf{\Omega}' p_{HG}(\mathbf{\Omega}\cdot\mathbf{\Omega}') P_L(\mathbf{\Omega}\cdot\mathbf{\Omega}') \sim \sum_{l'=1}^{N_\Omega} w_{l'} p_{ll'} P_L(\mathbf{\Omega}_l\cdot\mathbf{\Omega}_{l'}). \tag{6}$$

A quadrature set of $\{w_l, \mathbf{\Omega}_l\}$ requires selecting for the DOM, so that many kinds of quadrature sets have been developed to satisfy a certain symmetry (Fiveland, 1991; Carlson, 1971; Balsara, 2001; Endo and Yamamoto, 2007; Lebedev, 1975, 1977). Among them, we used the level symmetric even (LSE) quadrature set (Fiveland, 1991), and the even and odd (EO) quadrature set (Endo and Yamamoto, 2007) because their superiorities were reported by several papers (Gregersen and York, 2005; Sanchez, 2012; Long et al., 2016; Fujii et al., 2018). Table 1 lists several numbers of the order, N_n, and total numbers, N_Ω, of both the quadrature sets, where N_n corresponds to the order of the Legendre polynomials for the LSE quadrature set and N_Ω is given by $N_n(N_n + 2)$ for both the sets. Hereafter , we use abbreviations of the two quadrature sets with the order of N_n, as LSEN_n and EON_n, respectively, *e.g.*, LSE6 means the LSE quadrature set with $N_n = 6$. The distributions of $\{w_l, \mathbf{\Omega}_l\}$ vary with the type and order of the quadrature sets, and resultantly the numerical errors of the scattering integral (Eq. (5)) and moment conditions (Eq. (6)) depend on the quadrature sets. For highly forward-peaked scattering, the dependence of the numerical errors on the quadrature sets is enhanced due to the exponential increase in the phase function toward the forward direction ($\mathbf{\Omega}\cdot\mathbf{\Omega}' = 1.0$) while the distribution of $\{w_l, \mathbf{\Omega}_l\}$ is independent of the form of the phase function, $p(\mathbf{\Omega}\cdot\mathbf{\Omega}')$, or the anisotropy factor, g. Hence, an appropriate numerical treatment of the highly forward-peaked phase function is crucial for accurate calculations of the RTE.

Table 1. List of the orders, N_n, and the total number of discrete angular directions, N_Ω, of the LSE (Fiveland, 1991) and EO (Endo and Yamamoto, 2007) quadrature sets. N_Ω is given by $N_n(N_n + 2)$.

$(w_l, \mathbf{\Omega}_l)$	$N_n(N_\Omega)$						
LSE	6(48)	8(80)	10(120)	12(168)	14(224)	16(288)	18(360)
EO	6(48)	8(80)	10(120)	12(168)	14(224)	16(288)	-

3.2. Finite order Legendre expansion (FL) method

For reduction of the numerical errors of the moment conditions (Eq. (6)), the expansion form of the phase function (Eq. (3)) is preferred to the original form (Eq. (2)) thanks to the orthogonality of the polynomials. The FL method approximates the phase function by a finite series of Legendre polynomials up to the order, N:

$$p_{FL}^N(\mathbf{\Omega} \cdot \mathbf{\Omega}') = \sum_{n=0}^{N} \frac{2n+1}{4\pi} \sigma_{n,\,HG} P_n(\mathbf{\Omega} \cdot \mathbf{\Omega}'). \tag{7}$$

Clearly, the truncated expansion of the phase function, $p_{FL}^N(\mathbf{\Omega} \cdot \mathbf{\Omega}')$ satisfies the L-th order moment conditions (Eq. (4)) for $0 \leq L \leq N$, while it does not for $L > N$. Figure 2(a) shows $p_{FL}^N(\mathbf{\Omega} \cdot \mathbf{\Omega}')$ as a function of $\mathbf{\Omega} \cdot \mathbf{\Omega}'$ in a logarithmic scale with different expansion orders, N, for $g = 0.9$. As N increases, the profile of $p_{FL}^N(\mathbf{\Omega} \cdot \mathbf{\Omega}')$ converges to that of $p_{HG}(\mathbf{\Omega} \cdot \mathbf{\Omega}')$ (Eq. (2)). However, the convergence of p_{FL}^N is slow for highly forward-peaked scattering when compared with that for isotropic scattering. Also, $p_{FL}^N(\mathbf{\Omega} \cdot \mathbf{\Omega}')$ has unphysical negative values due to the Legendre polynomial expansion. Such negative values do not appear in the renormalization methods, where the phase function is not expanded.

It is noted that if the truncated expansion of the phase function is accurate, there is no need to use special techniques for highly forward-peaked scattering. Nonetheless, the convergence of the truncated expansion is not necessarily important. More important for highly forward-peaked scattering is the numerical accuracy of the discrete scattering integral (right hand side of Eq. (5)) with adequate discrete angular directions (Morel, 1979).

For numerical calculations, the phase function is formulated in a matrix form, and the matrix in the case of the FL method is denoted as $\boldsymbol{p}_{FL}^N$ with a size of $N_\Omega \times N_\Omega$. In this paper, we employed the zeroth order renormalization method, developed by Liu and co-workers (Liu et al., 2002), to $\boldsymbol{p}_{FL}^N$, and it is denoted by $\hat{\boldsymbol{p}}_{FL}^N$. By the zeroth order renormalization method, $\hat{\boldsymbol{p}}_{FL}^N$ includes the weights of the quadrature sets, w_l.

3.3. delta-Eddington (dE) method

The dE method, also called as the delta-M method ("M" implies "moment") or the extended transport correction , decomposes the highly forward-peaked phase function into a purely forward-peaked component, expressed by the delta function and other component (Joseph et al., 1976; Welch and van Gemert, 1995; Morel, 1979):

$$p_\delta^M(\mathbf{\Omega} \cdot \mathbf{\Omega}') = \frac{1}{2\pi} h\delta(1 - \mathbf{\Omega} \cdot \mathbf{\Omega}') + (1-h) p_{\delta 2}^M(\mathbf{\Omega} \cdot \mathbf{\Omega}'), \tag{8}$$

where h is a coefficient of the decomposition. $p_{\delta 2}^M$ is a phase function excluding the delta-function component and expanded in a finite series of Legendre polynomials up to the order of M:

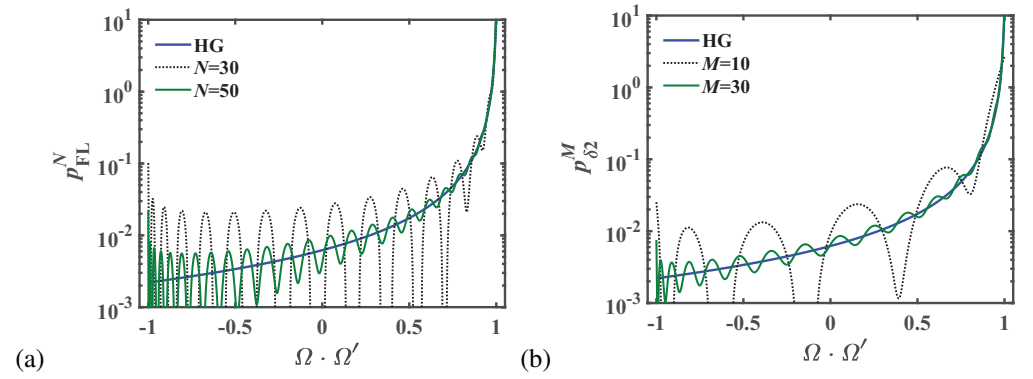

Fig. 2. The phase functions for $g = 0.9$, (a) p_{FL}^N (Eq. (7)) using the FL method at the expansion orders $N = 30$ and 50; and (b) $p_{\delta 2}^M$ (Eq. (9)) using the dE method at $M = 10$ and 30. The negative values of the phase functions are replaced by 10^{-4}. p_{HG} (Eq. (2)) is plotted as a reference.

$$p_{\delta 2}^M(\boldsymbol{\Omega} \cdot \boldsymbol{\Omega}') = \sum_{n=0}^{M} \frac{2n+1}{4\pi} \sigma_{n,\,dE} P_n(\boldsymbol{\Omega} \cdot \boldsymbol{\Omega}'). \tag{9}$$

In the case of the HG phase function, the expansion coefficient, $\sigma_{n,\,dE}$, is determined so as to satisfy the moment conditions up to the order of $M + 1$:

$$\sigma_{n,\,dE} := \int_{\mathbb{S}^2} d\boldsymbol{\Omega}' p_{\delta 2}^M(\boldsymbol{\Omega} \cdot \boldsymbol{\Omega}') P_n(\boldsymbol{\Omega} \cdot \boldsymbol{\Omega}') = \frac{g^n - h}{1 - h}, \qquad h = g^{M+1}. \tag{10}$$

It is noted that determination of h is arbitrary when the moment conditions are satisfied up to the order of M, although we determined h from the (M+1)-th order moment condition. The case of $n = 0$ in Eq. (10) corresponds to the normalization condition of $p_{\delta 2}^M$: $\int_{\mathbb{S}^2} d\boldsymbol{\Omega}' p_{\delta 2}^M(\boldsymbol{\Omega} \cdot \boldsymbol{\Omega}') = 1$. By using p_δ^M (Eq. (8)), the RTE (Eq. (1)) is approximated to

$$\left[\frac{\partial}{v \partial t} + \boldsymbol{\Omega} \cdot \nabla + \mu_a(\boldsymbol{r}) + \mu_s^M(\boldsymbol{r}) \right] I(\boldsymbol{r}, \boldsymbol{\Omega}, t) = \mu_s^M(\boldsymbol{r}) \int_{\mathbb{S}^2} d\boldsymbol{\Omega}' p_{\delta 2}^M(\boldsymbol{\Omega} \cdot \boldsymbol{\Omega}') I(\boldsymbol{r}, \boldsymbol{\Omega}', t) + q(\boldsymbol{r}, \boldsymbol{\Omega}, t), \tag{11}$$

where $\mu_s^M(\boldsymbol{r}) = (1 - h)\mu_s(\boldsymbol{r}) = (1 - g^{M+1})\mu_s(\boldsymbol{r})$. Equation (11) means that μ_s is modified to μ_s^M by the delta-function component and that the phase function is replaced by $p_{\delta 2}^M$. Hence, we investigated mainly $p_{\delta 2}^M$ rather than p_δ^M for the dE method. Figure 2(b) shows that $p_{\delta 2}^M$ converges to p_{HG} faster than p_{FL}^N with the increase in the order M or N. Similarly to the case of the FL method, we renormalized the phase function for the dE method, denoted by $\hat{\boldsymbol{p}}_{\delta 2}^M$ in a matrix form.

3.4. Galerkin quadrature (GQ) method

The GQ method expands the phase function in a finite series of Legendre polynomials, as well as the FL method does. In addition, this method conducts the weighting procedure to the highly forward-peaked phase function by requiring that the residual of the scattering integral is orthogonal to the weighting space, spanned by the spherical harmonics. Because the spherical harmonics are eigenfunctions of the analytic scattering operator, the GQ method can construct accurately the discrete scattering integral corresponding to the interpolation of the discrete light intensities with a given quadrature set by the spherical harmonics. Here, the analytic scattering operator, $\mathscr{L}_s$, is defined as

$\mathscr{L}_s I(\boldsymbol{r}, \boldsymbol{\Omega}, t) = \mu_s(\boldsymbol{r}) \int_{\mathbb{S}^2} d\boldsymbol{\Omega}' p(\boldsymbol{\Omega} \cdot \boldsymbol{\Omega}') I(\boldsymbol{r}, \boldsymbol{\Omega}', t)$; and the eigenvalue for the spherical harmonics of degree n and order m, Y_n^m, is the expansion coefficient σ_n for the phase function in the Legendre polynomial of degree n. Hence, if a quadrature set is adequately chosen to represent the discrete light intensity, the GQ method can provide the accurate solution of the RTE, regardless of the convergence of the truncated expansion of the phase function by Legendre polynomials. For the details, please refer the original papers (Morel, 1989; Morel et al., 2017). In the GQ method, the phase function matrix, $\hat{\boldsymbol{p}}_G$, with a size of $N_\Omega \times N_\Omega$, is formulated as

$$\hat{\boldsymbol{p}}_G = \boldsymbol{M}\boldsymbol{\Sigma}\boldsymbol{D}, \tag{12}$$

where $\boldsymbol{M}$ is the moment-to-direction matrix, $\boldsymbol{\Sigma}$ the cross section matrix, and $\boldsymbol{D}$ the direction-to-moment matrix, respectively. We numerically calculated $\hat{\boldsymbol{p}}_G$ based on the numerical code developed in our previous paper (Fujii et al., 2018). Element of $\boldsymbol{M}$, M_{ld}, in 3D is given by the spherical harmonics:

$$M_{ld} = Y_n^m(\boldsymbol{\Omega}_l), \qquad l = 1, 2, \cdots, N_\Omega, \qquad d = 0, 1, \cdots, N_\Omega - 1, \tag{13}$$

where $\boldsymbol{\Omega}_l$ denotes the l-th discrete angular direction; and d corresponds to a combination of indices of n and m, sorted in an arbitrary numbering order, *e.g.*, $d = 0$ for $(n, m) = (0, 0)$, $d = 1$ for $(n, m) = (1, -1)$, and so on. The maximum degree of the spherical harmonics depends on the quadrature order, N_n. For LSEN_n and EON_n, the maximum degree is determined as $N_n + 1$ to interpolate the weighting space. This is because that the quadrature set in 3D, LSEN_n or EON_n, has more directions than the number of the spherical harmonics of degree $N_n - 1$, requiring the certain additional spherical harmonics of degrees N_n and $N_n + 1$, and the exclusion of all other spherical harmonics. $\boldsymbol{D}$ is calculated by inversion of $\boldsymbol{M}$ based on the requirement of the GQ method, $\boldsymbol{M}\boldsymbol{D} = \boldsymbol{E}$, with the unit matrix, $\boldsymbol{E}$. $\boldsymbol{\Sigma}$ is a diagonal matrix consisting of the expansion coefficients of the phase function, $\sigma_{n,HG}$, at the degree $n \in [0, 1, \cdots N_n + 1]$ (Eq. (4)). The components of $\boldsymbol{\Sigma}$ are sorted so that the degree, n, of $\sigma_{n,HG}$ is equivalent to the degree, n, of the spherical harmonics in $\boldsymbol{M}$ and $\boldsymbol{D}$.

3.5. Conjunction of the GQ method with the dE method: the GQ-dE method

We considered the conjunction of the GQ method with the dE method, called as the GQ-dE method, by the simple modification of the cross section matrix, $\boldsymbol{\Sigma}$, in Eq. (12). In the GQ-dE method, the phase function matrix, $\hat{\boldsymbol{p}}_{Gd}$, with a size of $N_\Omega \times N_\Omega$, is formulated as

$$\hat{\boldsymbol{p}}_{Gd} = \boldsymbol{M}\boldsymbol{\Sigma}_{dE}\boldsymbol{D}, \tag{14}$$

where $\boldsymbol{M}$ and $\boldsymbol{D}$ are the same as those in $\hat{\boldsymbol{p}}_G$ (Eq. (12)), and $\boldsymbol{\Sigma}_{dE}$ consists of the expansion coefficients based on the dE method, $\sigma_{n,dE}$, at the degree $n \in [0, 1, \cdots N_n + 1]$ (Eq. (10)) with $h = g^{N_n+2}$. The RTE using the GQ-dE method in angular discretization is given as

$$\left[\frac{\partial}{v\partial t} + \boldsymbol{\Omega}_l \cdot \nabla + \mu_a(\boldsymbol{r}) + \mu_s^{N_n+1}(\boldsymbol{r})\right] I_l(\boldsymbol{r}, t) = \mu_s^{N_n+1}(\boldsymbol{r}) \sum_{l'=1}^{N_\Omega} (\hat{\boldsymbol{p}}_{Gd})_{ll'} I_{l'}(\boldsymbol{r}, t) + q_l(\boldsymbol{r}, t). \tag{15}$$

3.6. Numerical errors of the L-th order moment conditions of the phase function

We examined the four kinds of methods for the highly forward-peaked phase function by the mean absolute percentage errors, e_L, of the L-th order moment condition: $\sigma_{L,HG} = g^L$ of Eq. (4) or $\sigma_{L,dE} = (g^L - h)/(1 - h)$ of Eq. (10). For the FL and GQ methods, e_L is defined as

$$
\begin{aligned}
e_L &= N_\Omega^{-1} \sum_{l=1}^{N_\Omega} |S_L^l - 1| \times 100, \qquad S_L^l = \sigma_{L,HG}^{-1} \sum_{l'=1}^{N_\Omega} \hat{p}_{ll'} P_L(\boldsymbol{\Omega}_l \cdot \boldsymbol{\Omega}_{l'}), \\
\hat{p}_{ll'} &= \begin{cases} \left(\hat{\boldsymbol{p}}_{FL}^N\right)_{ll'} & \text{for the FL method} \\ (\hat{\boldsymbol{p}}_G)_{ll'} & \text{for the GQ method} \end{cases}.
\end{aligned} \tag{16}
$$

For the dE and GQ-dE methods, we need to define e_L in the following two cases because of $\sigma_{L,dE} = 0$ at $L = M + 1$ for the dE method and at $L = N_n + 2$ for the GQ-dE method, respectively:

$$
\begin{aligned}
e_L &= \begin{cases} N_\Omega^{-1} \sum_{l=1}^{N_\Omega} |S_L^l| \times 100, & S_L^l = \sum_{l'=1}^{N_\Omega} \hat{p}_{ll'} P_L(\boldsymbol{\Omega}_l \cdot \boldsymbol{\Omega}_{l'}) \quad (L = M + 1 \text{ or } L = N_n + 2) \\ N_\Omega^{-1} \sum_{l=1}^{N_\Omega} |S_L^l - 1| \times 100, & S_L^l = \sigma_{L,dE}^{-1} \sum_{l'=1}^{N_\Omega} \hat{p}_{ll'} P_L(\boldsymbol{\Omega}_l \cdot \boldsymbol{\Omega}_{l'}) \quad \text{(otherwise)} \end{cases}, \\
\hat{p}_{ll'} &= \begin{cases} \left(\hat{\boldsymbol{p}}_{\delta 2}^M\right)_{ll'} & \text{for the dE method} \\ (\hat{\boldsymbol{p}}_{Gd})_{ll'} & \text{for the GQ} - \text{dE method} \end{cases}.
\end{aligned} \tag{17}
$$

4. Numerical schemes and conditions for the RTE-calculations

4.1. Finite difference method

In numerical calculations of the RTE based on the FL, dE, GQ, and GQ-dE methods, we employed the finite difference method: the 3rd order weighted essentially non oscillatory scheme (Jiang and Shu, 1996; Henrick et al., 2005) for spatial discretization and the 3rd order total variation diminishing-Runge-Kutta method (Gottlieb and Shu, 1998) for temporal discretization, respectively. For the details, refer to (Fujii et al., 2018).

4.2. Numerical phantom modeling biological tissue volumes

As a first step toward the numerical calculations of the RTE in heterogeneous biological tissue volumes, we consider a homogeneous numerical phantom because analytical solutions of the RTE are available for homogeneous media. The phantom is a cubic medium with a side of 2.2 cm as shown in Fig. 3. The source and detector are located inside the medium at $\boldsymbol{r}_s$ = (1.10 cm, 1.10 cm, 0.88 cm) and $\boldsymbol{r}_d = \boldsymbol{r}_s + \rho\hat{\boldsymbol{e}}_z$, respectively, with the source-detector (SD) distance of ρ; and the unit vector of z-axis of $\hat{\boldsymbol{e}}_z$ for the purpose of suppressing boundary effects because we compare the numerical calculations for finite media with the analytical solution for infinite media. At the boundary of a medium, the non-reentry boundary condition is employed for simplicity. It was confirmed that the boundary condition little influences the numerical calculation of the RTE at the detector inside the medium. The optical properties of the phantom were given as $\mu_s = 100$ cm^{-1}, $\mu_a = 0.2$ cm^{-1}, $g = 0.9$, and the refractive index $n = 1.4$. These values are typical for biological tissues in the near-infrared wavelength range.

4.3. Numerical conditions and computational loads

We calculated temporal profiles of the fluence rate, $\Phi(\boldsymbol{r}_d, t) = \int_{\mathbb{S}^2} d\boldsymbol{\Omega} I(\boldsymbol{r}_d, \boldsymbol{\Omega}, t)$ from the RTE solution using the FL, dE, GQ, and GQ-dE methods in the time range from 0 to 350 ps. In the numerical calculation of $\Phi \sim \sum_{l=1}^{N_\Omega} w_l I_l$ using the GQ and GQ-dE methods, we have two choices of the weight, w_l; the weight for the quadrature set or the companion weight, which corresponds to the first row components of $\boldsymbol{D}$ (Morel et al., 2017). We preliminarily confirmed that the Φ-results were almost the same between the two cases for the weights. The spatial and temporal step sizes were uniformly given as $\Delta r = 0.02$ cm and $\Delta t = 0.5$ ps, respectively. The preliminary study showed that Φ was little changed when the step sizes were finer than the current values. The source code for the numerical calculation was written in the C++ programming language, and all the matrices were compressed to vectors in the compressed row storage format. Also, parallel CPU programming was implemented with 48 thread computers (Intel Xeon E5-2690v3@ 2GHz) by using OpenMP. The numerical code for the RTE-calculations is available as an open source (Fujii, 2020). In this work, the total numbers of spatial nodes and time steps, N_r and N_t, were the same among the four numerical treatments of the highly forward-peaked phase function. Hence, the memory requirements and computational loads were directly related to the N_Ω-values, which ranges from 48 to 288 for the LSE and EO quadrature sets as listed in Table 1. In the case of $N_\Omega = 48 (N_n = 6)$, the operator matrix size ($N_r N_\Omega \times N_r N_\Omega$) of 2.5×10^{15} and CPU times of 5.2 hours were the smallest among the N_Ω-range (N_n-range) listed in Table 1. Meanwhile, in the case of $N_\Omega = 288 (N_n = 16)$, they were the largest as 1.4×10^{17} and 34.9 hours, respectively. Resultantly, LSE6 is computationally more efficient than LSE16: the computation time of the RTE calculation with LSE6 was one-seventh of that with LSE16. Dependency of the computational times and costs of the RTE-calculations on the spatial and temporal resolutions, Δr and Δt, will be discussed elsewhere by changing the values of Δr and Δt.

4.4. Numerical errors of the fluence rate for the time-dependent RTE

We investigated the accuracy of the numerical calculations of the time-dependent RTE using the FL, dE, GQ, and GQ-dE methods by comparing with the analytical solution of the RTE for infinite homogeneous media with the highly forward-peaked scattering (Liemert and Kienle, 2012). The differences in Φ between the numerical and analytical solutions were evaluated by the mean absolute percentage error, e_Φ, of the fluence rate normalized by its peak value, $\hat{\Phi} = \Phi / \max(\Phi)$:

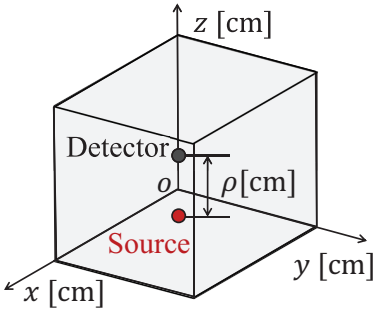

Fig. 3. Source and detector positions in the homogeneous cubic phantom

$$e_\Phi = \frac{1}{M_2 - M_1} \sum_{m=M_1}^{M_2} \left| \frac{\hat{\Phi}^m - \hat{\Phi}_{RTE}(t_m)}{\hat{\Phi}_{RTE}(t_m)} \right| \times 100, \tag{18}$$

where $\hat{\Phi}^m$ and $\hat{\Phi}_{RTE}(t_m)$ represent the values of $\hat{\Phi}$ at the m-th time step, t_m, in the numerical and analytical solutions, respectively; and the summation with respect to m is over the time period from the time when $\hat{\Phi}_{RTE}$ rises to $10^{-0.5} \backsimeq 0.316$ ($m = M_1$) before the peak to the time when $\hat{\Phi}_{RTE}$ falls to $10^{-1.5} \backsimeq 0.032$ ($m = M_2$) after the peak. For the details of the time period, please refer to (Fujii et al., 2018).

4.5. Determination of the source-detector (SD) distance

As mentioned in Introduction, we examined the RTE-calculations using the FL, dE, GQ, and GQ-dE methods in the region of the scattering length scale, where the highly forward-peaked phase function strongly influences the results for the RTE. Under the current conditions of the optical properties, we determined the SD distance, ρ, as 0.40 cm by our preliminary study using three kinds of analytical solutions: (1) the RTE (Liemert and Kienle, 2012) with appropriate treatments of the highly forward-peaked phase function; (2) the RTE using the zeroth order dE method (Eq. (11) at $M = 0$, denoted by dE0), which approximates the phase function as the delta-function and isotropic scattering components; and (3) the diffusion equation (DE) (Chandrasekhar, 1943) which assumes isotropic scattering under the diffusion approximation.

Figures 4(a) and (b) show the temporal profiles of the three kinds of analytical solutions: the RTE, dE0, and DE. At the short SD distance, $\rho = 0.40$ cm, the profiles of the dE0 and DE disagreed with that of the RTE, meaning the strong influences of the highly forward-peaked phase function. At the long SD distance, $\rho = 1.55$ cm, meanwhile, the profiles of the dE0 and DE almost agreed with that of the RTE, suggesting the validity of the isotopic scattering approximation to the highly forward-peaked phase function. From the results, the ρ-value of 0.40 cm is in the region of the scattering length scale, while the value of 1.55 cm in the region of the diffusive length scale. Although not shown here, our preliminary study showed that in the region of the scattering length scale, the temporal profiles of the analytical solutions of the RTE, dE0, and DE differed each other around the peak time if normalization by its maximum value is not employed. On the other hand, in the region of the diffusive length scale, the three profiles almost agreed even without the normalization.

5. Numerical results

5.1. Moment conditions of the highly forward-peaked phase function

This subsection discusses the numerical errors, e_L, of the L-th order moment conditions of the highly forward-peaked phase function (Eqs. (16) and (17)) for the FL, dE, GQ, and GQ-dE methods with the LSE and EO quadrature sets. For the FL and dE methods, the expansion orders, N and M, are given independently of the quadrature orders, N_n. Hence, their parameter spaces are given as $\{L, N_n, N\}$ and $\{L, N_n, M\}$, respectively. For the GQ and GQ-dE methods, meanwhile, the expansion order of the phase function is consistently determined according to the quadrature order. Hence, the parameter space is reduced to $\{L, N_n\}$ for the GQ and GQ-dE methods. Since the e_L-value of 1% is sufficiently small, we assume that the L-th order moment condition is satisfied when the e_L-value is less than 1% here.

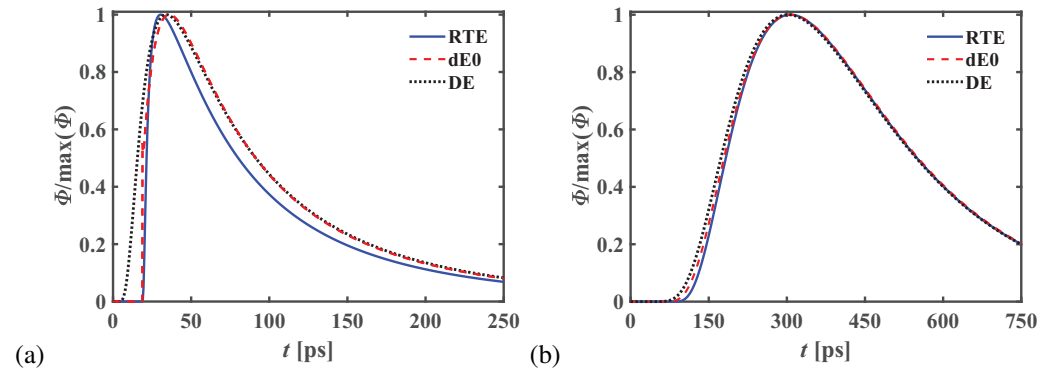

Fig. 4. Analytical solutions of the RTE, dE0 (Eq. (11) with $M = 0$), and DE at the short and long SD distances: (a) $\rho = 0.40$ cm and (b) $\rho = 1.55$ cm.

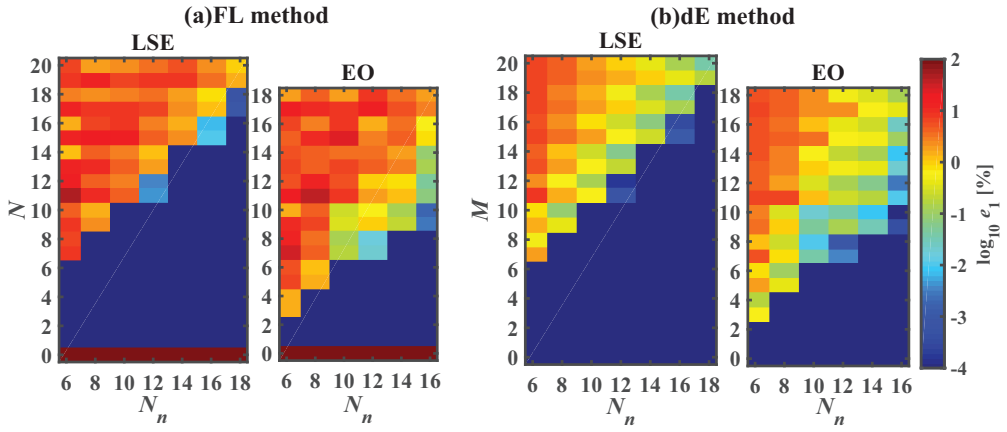

Fig. 5. Mapping of the mean absolute percentage errors, e_1, of the first order moment condition (Eqs. (16) and (17) with $L = 1$) for the (a) FL and (b) dE methods on the $N_n - N$ and $N_n - M$ planes with the LSE (left) and EO (right) quadrature sets in the case of $g = 0.9$. N_n represents the quadrature order; and N and M the expansion orders of the phase function. The e_1-values larger than 10^2% were replaced by 10^2%, and the e_1-values less than 10^{-4}% were replaced by 10^{-4}%.

We discuss the e_L-results at the range of $1 \leq L \leq 5$ for all the combinations of the treatments of the highly forward-peaked scattering (FL, dE, GQ, and GQ-dE methods), quadrature sets (LSE and EO sets), and the expansion orders. For most of the combinations, the errors are induced by the angular discretization using the DOM at the L-range. We preliminarily confirmed that the numerical errors at $L = 0$, e_0, were less than 1% for the FL and dE methods at all the combinations of the quadrature sets and expansion orders because the zeroth order renormalization method was employed. We mainly examined the numerical errors at $L = 1$, e_1, because a strong correlation between e_1 and e_Φ has been reported for the renormalization method (Fujii et al., 2018). Meanwhile, we do not discuss the e_L-values at the higher order $L \geq 6$ because these e_L-values are little correlated to the RTE-results.

5.1.1. First order moment condition of the phase function

Figures 5(a) and (b) show the maps of the e_1-results ($L = 1$) on the N_n-N and N_n-M planes for the FL and dE methods, respectively, where N_n varied from 6 to 18 for the LSE quadrature sets and from 6 to 16 with the EO quadrature sets as listed in Table 1; and both N and M varied from 0 to $N_n + 2$. For simplicity, the e_1-values larger than 10^2% were replaced by 10^2% and those smaller than 10^{-4}% by 10^{-4}%.

As shown in Fig. 5(a), the e_1-values at $N = 0$ for the FL method were quite large with the LSE and EO quadrature sets because the phase function using the FL method at $N = 0$, p^0_{FL}, theoretically does not satisfy the first order moment condition: $\int_{\mathbb{S}^2} d\boldsymbol{\Omega}'\boldsymbol{\Omega}\cdot\boldsymbol{\Omega}' p^0_{FL} = 0 \neq \sigma_{1,HG} = g$. At $N > 0$, the e_1-values for the FL method depended on both N_n and N, and the e_1-values did not decrease monotonically with the increase in N. For example, in the case of LSE6 ($N_n = 6$), the e_1-values were less than 1% at $0 < N \leq 6$, while those were larger than 1% at $N > 6$. This is probably because the quadrature order, N_n, represents the maximum order of the Legendre expansion with the quadrature set. Although the e_1-results with the EO quadrature set were similar to those with the LSE quadrature set, the region of the e_1-values less than 1% was narrower than that with the LSE quadrature set. These results suggest that the errors at $N \geq 1$ are caused by the angular discretization based on the DOM.

Figure 5(b) shows the maps of e_1 on the N_n-M planes for the dE method with the LSE and EO quadrature sets. Unlike the results for the FL method, the e_1-values at $M = 0$ are sufficiently small with both the quadrature sets because the phase function using the dE method at $M = 0$ theoretically satisfies the first order moment condition as given in Eq. (10). On the whole, the e_1-values for the dE method were smaller than those for the FL method with both the quadrature sets. This is probably because the dE method weakens the highly forward-peaked scattering by removing the purely forward-peaked component from the original phase function. However, the regions of the e_1-values less than 1% were almost the same between the FL and dE methods, because both the methods conduct the same weighting procedure of the zeroth order renormalization method.

5.1.2. L-th order moment condition of the phase function

Figures 6 (a) and (b) show the maps of e_2 ($L = 2$) on the N_n-N and N_n-M planes for the FL and dE methods, respectively. The e_2-values at $N = 0$ and 1 for the FL method and at $M = 0$ for the dE method were larger than 10^2%, independently of the quadrature sets, because the phase functions using the FL and dE methods do not satisfy the second order moment conditions theoretically at the expansion orders. Similarly to the e_1-results, the dE method reduced the e_2-values from those for the FL method at N or $M \geq 2$, dependently on the quadrature sets. Meanwhile, for the FL and dE methods, the regions of the e_2-values less than 1% at both the quadrature sets were narrower than those of the e_1-values. Although not shown here, we confirmed that as the order L is higher, the region of the e_L-values less than 1% becomes narrower.

We discuss the e_L-results for the GQ method at $0 \leq L \leq 5$ with the LSE and EO quadrature sets as shown in Fig. 7. The e_L-values were sufficiently small as 10^{-4}% for both the quadrature sets except the case of EO8 ($N_n = 8$) at $L = 4$ and 5. These results suggest that the GQ method effectively reduces the errors induced by angular discretization using the DOM from those for the FL method, almost regardless of the types and orders of the quadrature sets. We confirmed that for EO8, the diagonal elements of the $\boldsymbol{M}$-matrix in Eq. (12) were so small that generating the $\boldsymbol{D}$-matrix by inversion of the $\boldsymbol{M}$-matrix was difficult.

We investigated the e_L-results for the GQ-dE method as shown in Fig. 8. The e_L-values for the GQ-dE method were almost the same as those for the GQ method, meaning the high versatility and high accuracy of the GQ-dE method, although the components of the phase function matrices differed between the two methods. These results

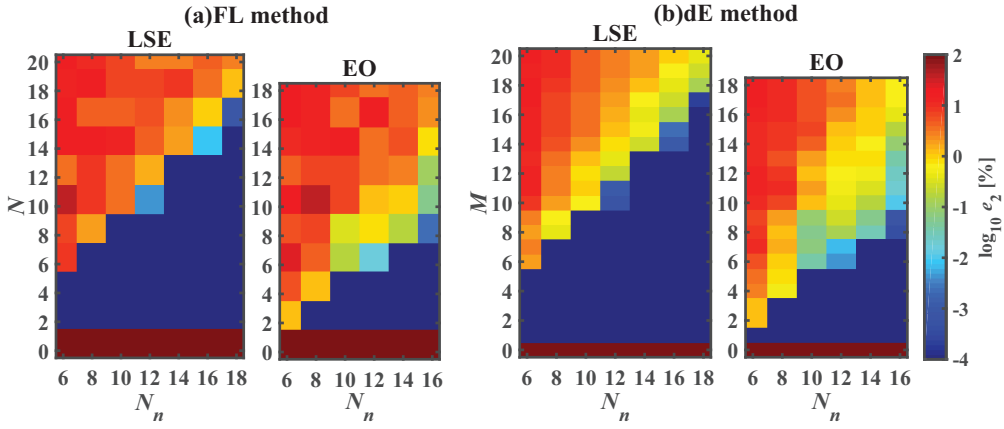

Fig. 6. Evaluation of the numerical errors, e_2, of the second order moment conditions (Eqs. (16) and (17) with $L = 2$) for the (a) FL and (b) dE methods. The other details are the same as Fig. 5.

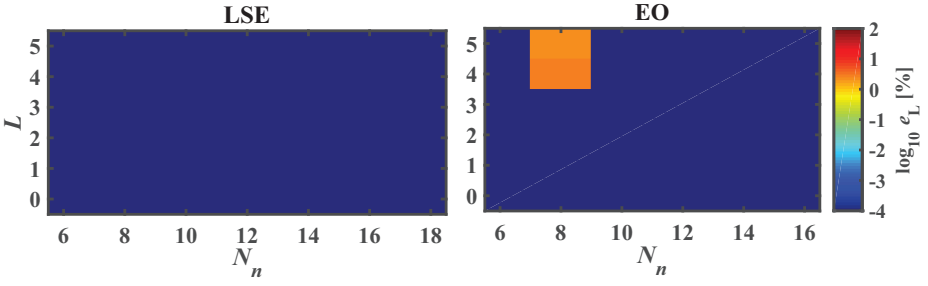

Fig. 7. Evaluation of the numerical errors, e_L, of the L-th order moment conditions (Eq. (16), $0 \le L \le 5$) for the GQ method at the N_n-range from 6 to 18 for the LSE quadrature set (left) and from 6 to 16 for the EO quadrature set (right). The other details are the same as in Fig. 6.

suggest that the matrices of $\boldsymbol{D}$ and $\boldsymbol{M}$ are more effective for the reduction of the errors than the modification of the cross section matrices to $\boldsymbol{\Sigma}_{dE}$ (Eq. (14)) from $\boldsymbol{\Sigma}$ (Eq. (12)).

5.2. Fluence rate

This subsection discusses the accuracy of the RTE-calculations using the FL, dE, GQ, and GQ-dE methods by the numerical errors, e_Φ, of the fluence rate (Eq. (18)) for the numerical phantom with $g = 0.9$ at the SD-distance of $\rho = 0.4$ cm in the region of the scattering length scale. For the FL and dE methods, we focus on the numerical results for LSE6 and EO6 because these combinations of the type and order of the quadrature sets are computationally more efficient than the other combinations. Then, we compare the results for LSE6 and EO6 with those for LSE16, which is supposed to provide the most accurate results.

Figure 9(a) shows the temporal profiles of $\Phi(\boldsymbol{r}_d, t)$ for the FL method with LSE6 at the expansion orders of the phase function: $N = 0$, 1, and 4. Although the numerical schemes and conditions for the spatial and temporal variables were the same in all the cases of the N-values, the RTE-results strongly depended on N. The top panel of Fig. 9(b) shows e_Φ for the FL method with LSE6 and EO6 at N ranging from 0 to 10, where the line of $e_\Phi = 2.18\%$ obtained by LSE16 is plotted as a reference. It is confirmed that the e_Φ-values with LSE16 were almost constant as 2.18% unless the RTE-results diverged. For LSE6, the e_Φ-values were less than 3% at $2 \le N \le 5$, and almost the same as the

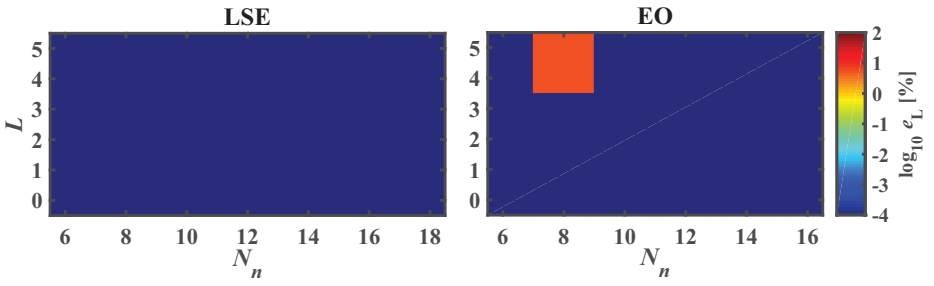

Fig. 8. Evaluation of the numerical errors, e_L, of the L-th order moment conditions (Eq. (16) for the GQ-dE method at LSEN_n (left) and EON_n (right). The other details are the same as in Fig. 7.

e_Φ-value with LSE16. Meanwhile, the e_Φ-values were larger than 3% at $N = 0$ and 1, and the RTE-results diverged at $6 \leq N \leq 10$. The divergence was probably caused by the fact that the phase function matrix using the FL method has many negative components. This behavior of the e_Φ-results was similar to that of the e_1-results shown in the bottom panel of Fig. 9(b).

As shown in Figs. 10(a) and (b), the dE method improved the accuracy of the RTE-calculations from that for the FL method, similarly to the e_1-results. Especially, in the case of LSE6, the e_Φ-values were less than 3% at $1 \leq M \leq 6$, almost the same accuracy as those with LSE16 indicated by the horizontal line. This result is consistent with the previous work by Klose and coworkers (Klose et al., 2005). They stated that the dE method with the second order expansion ($M = 2$) provided the accurate results of the steady-state RTE, and the expansion order ($M = 2$) is within the above range of $1 \leq M \leq 6$ with the small e_Φ-values. At $M = 0$, the e_Φ-value was as large as approximately 20% with LSE6 and EO6, although e_1-values were as small as 10^{-4}%. This is ascribed to the shape difference in the phase function between the zeroth order dE and the original HG form. The RTE-results for the dE method did not diverge with LSE6 and EO6 unlike the results for the FL method, although the e_1-values for the dE method were as large as approximately 5% at $7 \leq M \leq 10$. This is probably because the dE method reduces the number of the negative components of the phase function matrix.

Figure 11(a) shows that the numerical results of $\Phi(\boldsymbol{r}_d, t)$ using the GQ method for LSE6, EO6, and LSE16 agreed well with the analytical solution of the RTE, indicating the high accuracy of the GQ method. As shown in the top panel of Fig. 11(b), all the results of e_Φ for the GQ method were less than 3%, independently of the type and order of the quadrature sets, similarly to the e_1-results shown in the bottom panel of Fig. 11(b). These results suggest the versatility and usefulness of the GQ method. We probably do not need preliminary investigations for the dependence of the RTE-results on the quadrature sets when we solve the RTE using the GQ method for other random media in future.

As shown in Fig. 12(a) and (b), the GQ-dE method provided the very accurate results for the RTE-calculations, similarly to the GQ method. The e_Φ-value with EO8 for the GQ-dE method was reduced from the value for the GQ method, probably because of the reduction of the scattering coefficient as seen in Eq. (15).

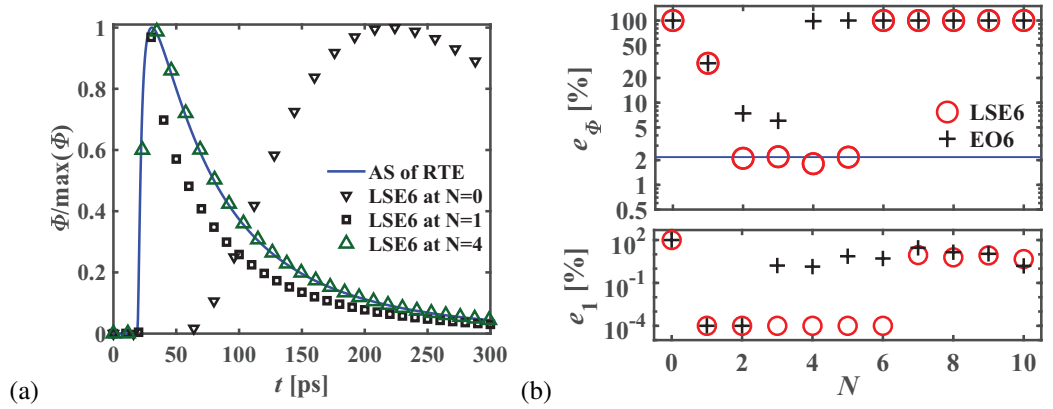

Fig. 9. (a) Temporal profiles of the fluence rate, $\Phi(\boldsymbol{r}_d, t)$, normalized by their peak values for the numerical phantom with $g = 0.9$ at ρ =0.40 cm; the numerical solutions of the RTE for the FL method with LSE6 at the expansion orders: $N = 0$, 1, and 4; and the analytical solution (AS) (Liemert and Kienle, 2012). (b, top) Numerical errors, e_Φ (Eq. (18)), for the FL method with LSE6 and EO6 at N ranging from 0 to 10 in a logarithmic scale. As a reference, the e_Φ-value of 2.18% obtained with LSE16 is plotted as a horizontal solid line. When the numerical solutions diverged or the e_Φ-values were larger than 100%, their values were replaced by 100%. (b, bottom) The e_1-results for the FL method are plotted for comparison with the e_Φ-results.

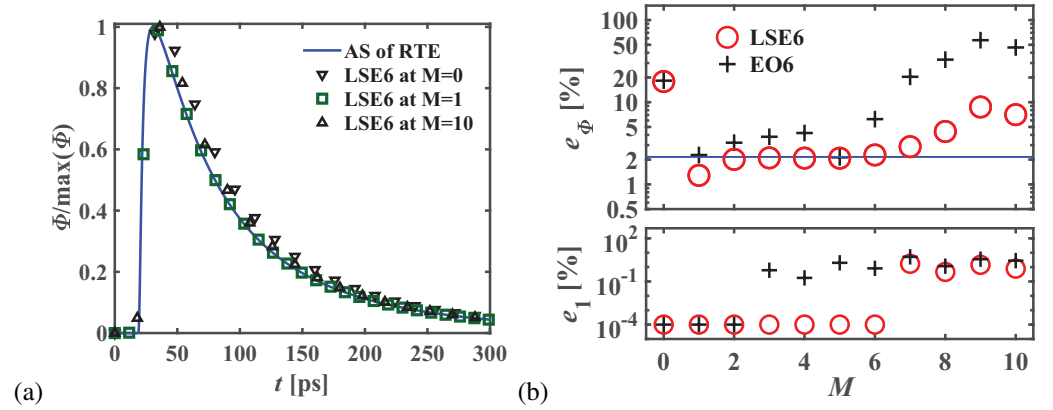

Fig. 10. Numerical results for the dE method: (a) $\Phi(\boldsymbol{r}_d, t)$ for LSE6 at $M = 0$, 1, and 10; and (b) e_Φ and e_1 at the M-range from 0 to 10. The other details are the same as in Fig. 9.

6. Conclusions

We examined the versatility and accuracy of the FL, dE, GQ, and GQ-dE methods with various expansion orders of the phase function and quadrature orders of the LSE and EO quadrature sets for the numerical treatments of the highly forward-peaked phase function in the 3D RTE based on the DOM. Firstly, we investigated the numerical errors, e_L, of the moment conditions of the highly forward-peaked phase function. We found that the dE method can reduce the e_L-values from those for the FL method, especially in the region where the large errors were caused by the breakdown of the moment condition of the phase function. This is because the dE method decomposes the phase function into the purely forward-peaked and other components. However, the reduction by the dE method depends on the expansion orders of the phase function and a type and order of the quadrature sets. The GQ method significantly reduced the errors, e_L, from those for the FL and dE methods in the region where the errors were caused by the angular discretization using the DOM. This large reduction by the GQ method is almost independent of a type and order of

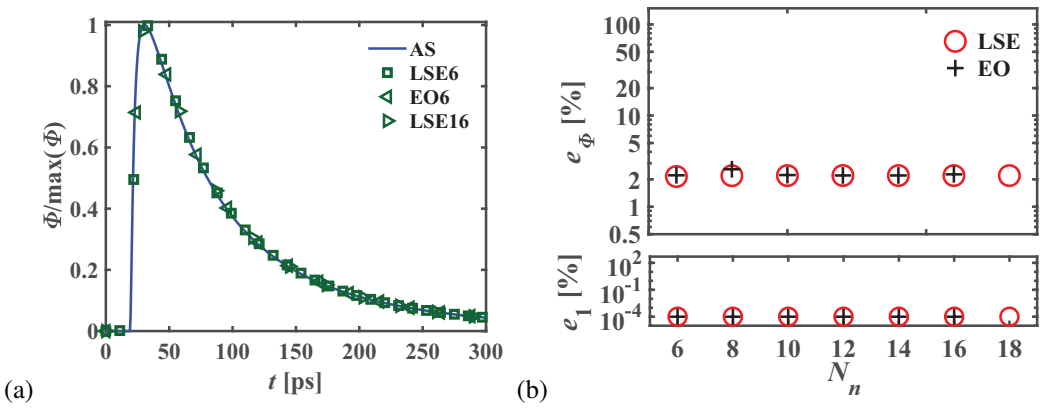

Fig. 11. Numerical results for the GQ method: (a) $\Phi(r_d, t)$ for LSE6, EO6, and LSE16; and (b) e_Φ and e_1 at the N_n-range from 6 to 18 for the LSE quadrature set and from 6 to 16 for the EO quadrature set. The other details are the same as in Fig. 9.

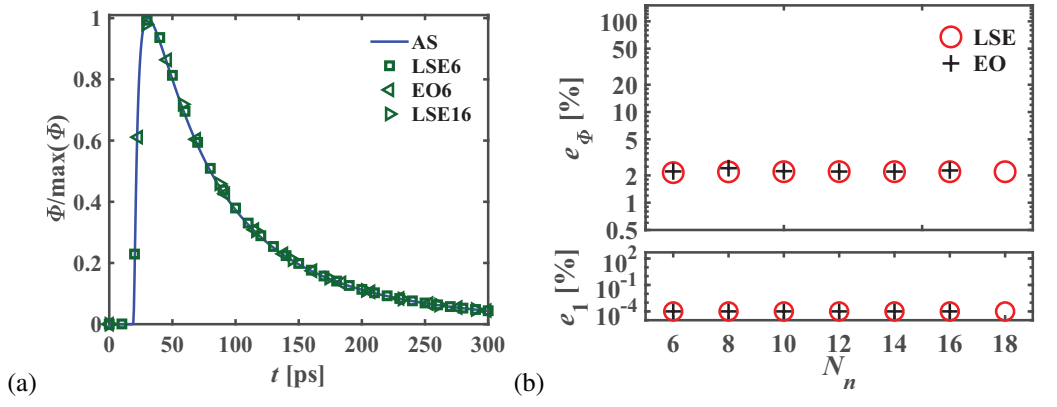

Fig. 12. Numerical results for the GQ-dE method. The other details are the same as in Fig. 11.

the quadrature sets because of the weighting procedure for the phase function according to the quadrature sets. The GQ-dE method provided the almost same accuracy as the GQ method. It suggests that the moment-to-direction and direction-to-moment matrices corresponding to the weighting procedure are more effective to the error reduction than the cross section matrices corresponding to the Legendre expansion of the phase function.

Secondly, we investigated the numerical calculations of the RTE for the highly forward-peaked scattering by the errors of the fluence rate, e_Φ, in the region of the scattering length scale, where the highly forward-peaked phase function strongly influences the RTE-results. When using the FL and dE methods, the e_Φ-values with LSE6 were less than 3%, the same accuracy with LSE16 at $2 \leq N \leq 5$ and $1 \leq M \leq 6$, respectively. These results suggest the accuracies of the FL and dE methods depend on the expansion orders. When using the GQ and GQ-dE methods, meanwhile, the e_Φ-values were less than 3% for all the types and orders of the quadrature sets investigated in this study, suggesting high versatility and usefulness of the GQ and GQ-dE methods.

In this paper, influences of the requirement of $\boldsymbol{MD} = \boldsymbol{E}$ for the GQ and GQ-dE methods on the numerical results have not been examined and will be discussed elsewhere. It is suggested that numerical errors in the eigenvalues of the scattering matrices would be correlated to the numerical accuracy of the discrete scattering integral or the

RTE-calculations for various kinds of treatments of the highly forward-peaked scattering, and the correlation will be discussed elsewhere.

Acknowledgments

This work was partially supported by JSPS KAKENHI Grant Numbers 18K13694, 18K18448, and 20H02076. H. Fujii would like to thank Drs. T. Endo, A. Yamamoto, and attendees at the 50th summer seminar of reactor physics division of the atomic energy society of Japan; and Ms. M. Ueno for fruitful discussion. He also would like to thank Dr. L. Tsang, his laboratory members, and staffs at University of Michigan for their kind supports to his research works. The authors would like to thank Reviewer #2 for the detailed comments of the GQ method and suggestion of the GQ-dE methods.

References

W. F. Cheong, S. A. Prahl, A. J. Welch, A review of the optical properties of biological tissue, IEEE J. Quantum Electron 26 (1990) 2166–2185.
L. Baranyai, M. Zude, Analysis of laser light propagation in kiwifruit using backscattering imaging and Monte Carlo simulation, Comput. Electron. Agric. 69 (2009) 33–39.
A. P. Gibson, J. C. Hebden, S. R. Arridge, Recent advances in diffuse optical imaging, Phys. Med. Biol. 50 (2005) R1–R43.
S. Okawa, Y. Hoshi, Y. Yamada, Improvement of image quality of time-domain diffuse optical tomography with lp sparsity regularization, Biomed. Opt. Express 2 (2011) 3334–3348.
R. Kannan, A. Przekwas, A computational model to detect and quantify a primary blast lung injury using near-infrared optical tomography, Int. J. Numer. Meth. Biomed. Engng. 27 (2011) 13–28.
Y. Yamada, S. Okawa, Diffuse Optical Tomography : Present Status and Its Future, Opt. Rev. 21 (2014) 185–205.
Y. Hoshi, Y. Yamada, Overview of diffuse optical tomography and its clinical applications, J. Biomed. Opt. 21 (2016) 091312.
J. H. Joseph, W. J. Wiscombe, J. A. Weinman, The delta-Eddington approximation for radioactive flux transfer, J. Atmos. Sci. 33 (1976) 2452–2459.
A. Welch, M. van Gemert, Optical-Thermal Response of Laser-Irradiated Tissue, Plenum Press, London, 1995.
A. D. Klose, V. Ntziachristos, A. H. Hielscher, The inverse source problem based on the radiative transfer equation in optical molecular imaging, J. Comput. Phys. 202 (2005) 323–345.
L. Liu, L. Ruan, H. Tan, On the discrete ordinates method for radiative heat transfer in anisotropically scattering media, Int. J. Heat Mass Transfer 45 (2002) 3259–3262.
B. Hunter, Z. Guo, Conservation of asymmetry factor in phase function discretization for radiative transfer analysis in anisotropic scattering media, Int. J. Heat Mass Transfer 55 (2012) 1544–1552.
F. Long, F. Li, X. Intes, S. P. Kotha, Radiative transfer equation modeling by streamline diffusion modified continuous Galerkin method, J. Biomed. Opt. 21 (2016) 036003.
H. Fujii, S. Okawa, Y. Yamada, Y. Hoshi, M. Watanabe, Renormalization of the highly forward-peaked phase function using the double exponential formula for radiative transfer, J. Math. Chem. 54 (2016) 2048–2061.
J. E. Morel, A Hybrid Collocation-Galerkin-Sn Method for Solving the Boltzmann Transport Equation, Nucl. Sci. Eng. 101 (1989) 72–87.
J. E. Morel, J. S. Warsa, B. C. Franke, A. K. Prinja, Comparison of Two Galerkin Quadrature Methods, Nucl. Sci. Eng. 185 (2017) 325–334.
H. Fujii, Y. Yamada, G. Chiba, Y. Hoshi, K. Kobayashi, M. Watanabe, Accurate and efficient computation of the 3D radiative transfer equation in highly forward-peaked scattering media using a renormalization approach, J. Comput. Phys. 374 (2018) 591–604.
J. Jia, H. K. Kim, A. H. Hielscher, Fast linear solver for radiative transport equation with multiple right hand sides in diffuse optical tomography, J. Quant. Spectrosc. Radiat. Transfer 167 (2015) 10–22.
A. D. Klose, A. H. Hielscher, Modeling Photon Propagation In Anisotropically Scattering Media With The Equation Of Radiative Transfer, Proc.SPIE 4955 (2003) 624–633.
S. Chandrasekhar, Radiative Transfer, Dover, New York, 1960.
L. G. Henyey, L. J. Greenstein, Diffuse radiation in the galaxy, J. Astrophys. 93 (1941) 70–83.
W. A. Fiveland, The selection of discrete ordinate quadrature sets for anisotropic scattering, ASME, HTD-vol. 160, Fundamentals of radiation heat transfer (1991) 89–96.
B. G. Carlson, Quadrature Tables of Equal Weight EQn Over the Unit sphere, Los Alamos Scientific Laboratory Report 4734 (1971).
D. Balsara, Fast and accurate discrete ordinates methods for multidimensional radiative transfer. Part I , basic methods, J. Quant. Spectrosc. Radiat. Transfer 69 (2001) 671–707.
T. Endo, A. Yamamoto, Development of New Solid Angle Quadrature Sets to Satisfy Even- and Odd-Moment Conditions, J. Nucl. Sci. Technol. 44 (2007) 1249–1258.
V. I. Lebedev, Values of the nodes and weights of ninth to seventeenth order gauss-markov quadrature formulae invariant under the octahedron group with inversion, USSR Comput. Math. Math. Phys. 15 (1975) 44–51.
V. I. Lebedev, Spherical quadrature formulas exact to orders 25-29, Siberian Math. J. 18 (1977) 99–107.
B. A. Gregersen, D. M. York, High-order discretization schemes for biochemical applications of boundary element solvation and variational electrostatic projection methods, J. Chem. Phys. 122 (2005) 194110.

R. Sanchez, Prospects in deterministic three-dimensional whole-core transport calculations, Nucl. Eng. Technol. 44 (2012) 113–150.

J. E. Morel, On the Validity of the Extended Transport Cross-Section Correction for Low-Energy Electron Transport, Nucl. Sci. Eng. 71 (1979) 64–71.

G.-S. Jiang, C.-W. Shu, Efficient Implementation of Weighted ENO Schemes, J. Comput. Phys. 126 (1996) 202–228.

A. K. Henrick, T. D. Aslam, J. M. Powers, Mapped weighted essentially non-oscillatory schemes: Achieving optimal order near critical points, J. Comput. Phys. 207 (2005) 542–567.

S. Gottlieb, C.-W. Shu, Total variation diminishing Runge-Kutta schemes, Math. Comp. 67 (1998) 73–85.

H. Fujii, Numerical codes for the time-dependent radiative transfer equation by FDM-DOM, 2020. URL: `https://data.mendeley.com/datasets/gb892bxd5j/2`. doi:10.17632/GB892BXD5J.2.

A. Liemert, A. Kienle, Infinite space Green's function of the time-dependent radiative transfer equation, Biomed. Opt. Express 3 (2012) 543.

S. Chandrasekhar, Stochastic Problems in Physics and Astronomy, Rev. Mod. Phys. 15 (1943) 1–88.